A Computationally Efficient Multi-Channel Multi-Pulse Coherent Fusion Algorithm for High-Speed Target Detection

Desheng Chen, Xiaolong Li, Mingxing Wang, Lingjie Guan, and Guolong Cui
School of Information and Communication Engineering
University of Electronic Science and Technology of China
Chengdu, China
Email: xiaolongliuestc@gmail.com

***Abstract*—Compared with the monostatic radar which only performs signal fusion in the multi-pulse dimension, the bistatic multiple-input multiple-output (MIMO) radar can also fuse multi-channel signals to improve the detection ability of high-speed moving targets. However, how to tackle the range migration (RM) caused by high-speed motion and compensate the signal difference between channels are the key problems in bistatic MIMO radar. To solve these problems, this paper proposes a computationally efficient multi-channel multi-pulse fusion algorithm. Firstly, we establish the echo model of bistatic MIMO radar with high-speed moving targets and utilize the Radon Fourier transform (RFT) algorithm to overcome the RM and complete the multi-pulse fusion. Then, the output characteristics of RFT, including peak and phase differences, are analyzed in detail. On this basis, a multi-channel coherent fusion method based on geometric information is proposed, which can eliminate the phase differences among channels and complete coherent fusion. Finally, numerical experiments show that the proposed algorithm can effectively detect the target under a low signal-to-noise ratio (SNR). Compared with the existing methods, the proposed algorithm can achieve a balance between computational complexity and detection performance.**

***Index Terms*—Bistatic multiple-input multiple-output (MIMO) radar, coherent fusion, range migration (RM), Radon Fourier transform (RFT).**

I. Introduction

With the advancement of stealth technology and aeronautics, an increasing number of high-speed, low-reflection targets, such as near-space vehicles and supersonic missiles, have emerged in recent years. The range migration (RM) [1]–[5] induced by the high-speed motion and low signal-to-noise ratio (SNR) resulted from low-reflection is challenging for target detection. As a novel radar paradigm, bistatic multiple-input multiple-output (MIMO) radar can improve the detection ability of such targets by transmitting orthogonal waveforms to conduct multi-channel signal fusion [6]–[9]. However, in order to enhance the detection performance of the high-speed low-reflection targets, the crucial issues are how to eliminate the RM and design an effective multi-channel fusion algorithm.

Many scholars have conducted excellent related research on the RM. Kong et al. [10] and Carlson et al. [11] introduced Radon transform (RT) and Hough transform (HT) methods to fuse the energy of each pulse in coherent processing interval (CPI), respectively. However, these two methods belong to incoherent fusion and do not use the phase information among pulses. The Keystone transform (KT) algorithm proposed by Perry et al. [12], [13] corrected the RM by transforming the slow time scale, but the algorithm requires interpolation operations, which often leads to gain loss. Xu et al. [14] proposed Radon Fourier transform (RFT), which extracts the target trajectory through Radon transform and constructs the corresponding Doppler filter bank. Further, the RFT could obtain the distinguished fusion gain.

To address the multi-channel signal fusion problem for bistatic MIMO radar, a fusion method with known target information is proposed in [15]. Nevertheless, it assumes that the target distance and velocity information are known, so the difference between channels can be compensated. In the case of unknown target information, Wang et al. [16] introduced a non-coherent fusion algorithm based on Cuckoo search, but it did not consider the RM problem caused by high-speed targets and ignored the phase relationship between channels, resulting in a loss of fusion performance. In addition, literature [17] has studied a high-speed target coherent fusion detection method. However, the algorithm jointly searches four dimensions, leading to a large amount of calculation and poor real-time performance. Therefore, how to efficiently realize high-speed target detection with bistatic MIMO is an urgent problem to be solved.

In this paper, we propose a multi-channel multi-pulse coherent fusion algorithm based on bistatic MIMO geometric information, which utilizes three search parameters and realizes the detection of high-speed targets under low SNR. Firstly, the echo model of the high-speed target observed by the bistatic MIMO radar system is established, and the RFT algorithm is used to complete the multi-pulse fusion. Then, the

This work was supported in part by the National Natural Science Foundation of China under Grant 62371113, in part by the Young Elite Scientists Sponsorship Program by CAST under Grant YESS20200082, in part by the Natural Science Foundation of Sichuan Province under Grant 2023NSFSC1386, and in part by the Aeronautical Science Foundation under Grant 2023Z017080001. (corresponding author: Xiaolong Li)

output characteristics of the RFT are analyzed. On this basis, a multi-channel coherent fusion approach based on geometric information is proposed. Numerical experiments present that the proposed algorithm is computationally effective compared with the existing methods.

II. Signal Model

This section provides the high-speed target's geometry model, transmitted signal, and received echo models for the bistatic coherent MIMO radar system.

A. Geometric Model

Fig. 1 depicts the bistatic short-baseline coherent MIMO radar system model. The radar system observes a far-field target, where d represents the distance between nodes. ρ_m^t and ρ_n^r are the radial distances between the target and the transmitted radar node $m(m=1,2)$ and the received radar node $n(n=1,2)$, respectively. The target travels at a constant speed of v in a horizontal direction, and the radial velocity of radar node m is v_m. The angle between node 1, node 2 and the target is ψ, and ϕ represents the observation angle of radar node 1. The instantaneous radial distance between the target and the radar nodes can be expressed as

$$\begin{cases} \rho_m^t(t_q) = \rho_m^t(0) + v_m t_q \\ \rho_n^r(t_q) = \rho_n^r(0) + v_n t_q \end{cases} \tag{1}$$

where $\rho_m^t(0) = \rho_m$ and $\rho_n^r(0) = \rho_n$ denote, respectively, the radial distance between the target and the transmitted node m and the received node n at the initial time, t_q denotes the slow time, and Q indicates the number of pulses within the CPI. The instantaneous radial distance in the $(m^t\text{-}n^r)$ (m-th transmitted node and n-th received node) channel can be represented as

$$\rho_{n,m}(t_q) = \rho_m^t(t_q) + \rho_n^r(t_q) = \rho_{n,m} + v_{n,m} t_q \tag{2}$$

where $\rho_{n,m} = \rho_m + \rho_n$ denotes the equivalent initial radial distance, whereas $v_{n,m} = v_n + v_m$ indicates the equivalent radial velocity along the $(m^t\text{-}n^r)$ channel.

B. Transmitted Signal Model

Each node utilizes orthogonal frequency division multiplexing-linear frequency modulation waveform (OFDM-LFM) and the signal transmitted by the m-th node is

$$s_m(t) = \sqrt{E}\,\mathrm{rect}\left(\frac{t}{T_p}\right)\exp\left(j2\pi\begin{pmatrix} f_c + (n-1)\Delta f \\ +0.5\mu t \end{pmatrix} t\right) \tag{3}$$

where t represents the fast time, E represents the transmitted energy, Δf represents the step frequency of the transmitted signal, $\mu = B/T_p$ represents the modulation slope, B stands for the LFM signal bandwidth, T_p denotes the pulse width and f_c denotes the carrier frequency, respectively.

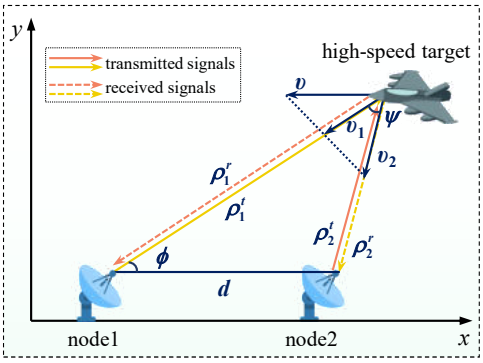

Fig. 1. Bistatic MIMO planar geometric model

C. Received Echo Model

Disregarding noise and clutter, the coupled echo received by the n-th node at the q-th pulse time can be represented as

$$\tilde{\vartheta}_n(t,t_q) = \sum_{m=1}^{2}\tilde{\vartheta}_{n,m}(t,t_q) = \sum_{m=1}^{2} s_m\left(t - \frac{\rho_{n,m}(t_q)}{c}\right) \tag{4}$$

where c denotes the speed of light. After down-conversion processing and utilize the matched filter $h_m(t) = s_m^*(-t)$ for matching and separating the n-th node's received coupled echo, after separation the echo of $(m^t\text{-}n^r)$ channel can be obtained

$$\begin{aligned}\vartheta_{n,m}(t,t_q) &= \int_{-\infty}^{\infty}\tilde{\vartheta}_n(\xi,t_q)\,h_m(t-\xi)\exp(-j2\pi f_c t)d\xi \\ &= E\,\mathrm{sin}\,c\left(B\left(t - \frac{\rho_{n,m}(t_q)}{c}\right)\right)\exp\left(-j2\pi f_m\frac{\rho_{n,m}(t_q)}{c}\right)\end{aligned} \tag{5}$$

where $\mathrm{sin}\,c(\cdot) = \sin(\pi x)/(\pi x)$ denotes the sinc function and $f_m = f_c + (m-1)\Delta f$ denotes the m-th node transmitted frequency. Substituting $\rho = c\tau$ into (5) yields

$$\begin{aligned}\vartheta_{n,m}(\rho,t_q) = E\,\mathrm{sin}\,c&\left(\frac{\rho - \rho_{n,m}(t_q)}{2\Delta\rho}\right) \\ &\times\exp\left(-j2\pi\frac{v_{n,m}t_q}{\lambda}\right)\exp\left(-j2\pi f_m\frac{\rho_{n,m}}{c}\right)\end{aligned} \tag{6}$$

where $\Delta\rho = c/2B$ represents the distance resolution, whereas $\lambda = c/f_c$ represents the wavelength of the original carrier frequency. When the step frequency Δf is significantly less than the carrier frequency f_c, then $\lambda = c/(f_c + (m-1)\Delta f) \approx c/f_c$ and the impact of the step frequency can be disregarded.

III. Multi-pulse Fusion

In this section, we use the RFT method to achieve multi-pulse fusion. In addition, the output characteristics of each channel fusion results are analyzed.

A. Multi-pulse Fusion based on RFT

Due to the negative impact of RM on the MTD's coherent performance, we utilize the RFT algorithm to aggregate

the energy of each pulse within CPI. The search parameters for range and speed in the RFT are represented as $[-\rho_{max}, \rho_{max}]$ and $[-\upsilon_{max}, \upsilon_{max}]$, respectively. The RFT searching unit for range and speed are indicated as $\Delta\rho = c/(2f_s)$ and $\Delta\upsilon = \lambda/(2QT_r)$, respectively. The RFT searching number of range and speed are, respectively, denoted as N_ρ =round$(2\rho_{max}/\Delta\rho)$, N_υ =round$(2\upsilon_{max}/\Delta\upsilon)$, where round$(\cdot)$ represents rounding. The discrete sequences used for searching distance and speed are as follows:

$$\rho_s(\alpha) = -\rho_{\max} + \alpha\Delta\rho, \quad \alpha = 1, 2, \ldots, N_\rho \tag{7a}$$

$$\upsilon_s(\beta) = -\upsilon_{\max} + \beta\Delta\upsilon, \quad \beta = 1, 2, \ldots, N_\upsilon \tag{7b}$$

The fusion output of (m^t-n^r) channel can be acquired by the RFT search

$$\begin{aligned}&\Omega_{n,m}\big(\rho_s(\alpha), \upsilon_s(\beta)\big)\\ &= \sum_{q=1}^{Q} E \sin c\left(\frac{\rho_s(\alpha) - \rho_s(\alpha^*_{n,m})}{2\Delta\rho} + \frac{\upsilon_s(\beta) - \upsilon_s(\beta^*_{n,m})}{2\Delta\rho} t_q\right)\\ &\times \exp\left(-j2\pi \frac{\upsilon_s(\beta) - \upsilon_s(\beta^*_{n,m})}{\lambda} t_q\right) \exp\left(-j2\pi f_m \frac{\rho_s(\alpha^*_{n,m})}{c}\right)\end{aligned} \tag{8}$$

where $\rho_s(\alpha^*_{n,m}) = \rho_n + \rho_m, \upsilon_s(\beta^*_{n,m}) = \upsilon_n + \upsilon_m$. Furthermore, if the RFT search parameters align with the target equivalent motion parameters, (8) can be approximately recast as

$$\begin{aligned}&\Omega_{n,m}\left(\rho_s(\alpha), \upsilon_s(\beta)\right)\\ &\approx QE \sin c\left(\frac{\rho_s(\alpha) - \rho_s(\alpha^*_{n,m})}{2\Delta\rho} + \frac{\upsilon_s(\beta) - \upsilon_s(\beta^*_{n,m})}{2\Delta\rho} t_q\right)\\ &\times \sin c\left(\frac{\upsilon_s(\beta) - \upsilon_s(\beta^*_{n,m})}{\lambda}\right) \exp\left(-j2\pi f_m \frac{\rho_s(\alpha^*_{n,m})}{c}\right)\end{aligned} \tag{9}$$

B. Output Characteristics

This section focuses on analyzing the RFT output properties of each channel, such as peak position and peak phase. According to (8), we can obtain the four channels output $\Omega_{1,1}, \Omega_{1,2}, \Omega_{2,1}$ and $\Omega_{2,2}$. The four RFT outputs' peak locations in the range dimension could be represented as $\rho_s(\alpha^*_{1,1}) = \rho_1 + \rho_1$, $\rho_s(\alpha^*_{2,1}) = \rho_1 + \rho_2$, $\rho_s(\alpha^*_{1,2}) = \rho_2 + \rho_1$ and $\rho_s(\alpha^*_{2,2}) = \rho_2 + \rho_2$, i.e. the peak position of the distance dimension is determined by the initial radial distance ρ_1 and ρ_2.

In the velocity dimension, the peak locations of the RFT outputs for the four channels could be written as $\upsilon_s(\beta^*_{1,1}) = \upsilon_1 + \upsilon_1$, $\upsilon_s(\beta^*_{2,1}) = \upsilon_1 + \upsilon_2$, $\upsilon_s(\beta^*_{1,2}) = \upsilon_2 + \upsilon_1$ and $\upsilon_s(\beta^*_{2,2}) = \upsilon_2 + \upsilon_2$, i.e. the peak position of the velocity dimension is determined by the target radial velocity υ_1 and υ_2. According to the four channels output, the peak phase can be obtained

$$p_{1,1} = \exp\left(-j2\pi f_1 \cdot \rho_s(\alpha^*_{1,1})/c\right) \tag{10a}$$

$$p_{2,1} = \exp\left(-j2\pi f_1 \cdot \rho_s(\alpha^*_{2,1})/c\right) \tag{10b}$$

$$p_{1,2} = \exp\left(-j2\pi f_2 \cdot \rho_s(\alpha^*_{1,2})/c\right) \tag{10c}$$

$$p_{2,2} = \exp\left(-j2\pi f_2 \cdot \rho_s(\alpha^*_{2,2})/c\right) \tag{10d}$$

substitute the peak locations in the range dimension into (10), we find the peak phase is related to the target initial radial distance ρ_1 and ρ_2.

Through the above analysis, we find that the output characteristics of RFT are determined by ρ_1, ρ_2, υ_1 and υ_2. Can we use fewer parameters to express the output characteristics discussed? According to Fig. 1, there are the following geometric relationships

$$\phi = \arccos\left((\rho_1^2 - \rho_2^2 + d^2)/(2\rho_1 d)\right) \tag{11a}$$

$$\psi = \arccos\left((\rho_1^2 + \rho_2^2 - d^2)/(2\rho_1\rho_2)\right) \tag{11b}$$

$$\upsilon_2 = \upsilon_1 \cos(\pi - \phi - \psi)/\cos\phi \tag{11c}$$

after some algebra, yields

$$\rho_2 = f_\rho\left(\rho_1, \phi\right) = \sqrt{\rho_1^2 + d^2 - 2d\rho_1\phi} \tag{12}$$

$$\upsilon_2 = f_\upsilon\left(\rho_1, \phi, \upsilon_1\right) = \upsilon_1 \frac{\cos\left(\phi + \cos^{-1}\left(\frac{\rho_1 - d\phi}{\rho_2}\right)\right)}{\cos\phi} \tag{13}$$

then the four RFT outputs' peak locations in the range dimension could be rewritten as

$$\rho_s(\alpha^*_{1,1}) = \rho_1 + \rho_1 = 2\rho_1 \tag{14a}$$

$$\rho_s(\alpha^*_{2,1}) = \rho_1 + \rho_2 = \rho_1 + f_\rho(\rho_1, \phi) \tag{14b}$$

$$\rho_s(\alpha^*_{1,2}) = \rho_2 + \rho_1 = f_\rho(\rho_1, \phi) + \rho_1 \tag{14c}$$

$$\rho_s(\alpha^*_{2,2}) = \rho_2 + \rho_2 = 2\rho_2 \tag{14d}$$

(14) shows that the peak position of the distance dimension is determined by the initial radial distance ρ_1 and the observation angle of node 1 ϕ. Similarly, the peak locations of the four RFT outputs in the velocity dimension could be rewritten as

$$\upsilon_s(\beta^*_{1,1}) = \upsilon_1 + \upsilon_1 = 2\upsilon_1 \tag{15a}$$

$$\upsilon_s(\beta^*_{2,1}) = \upsilon_1 + \upsilon_2 = \upsilon_1 + f_\upsilon(\rho_1, \phi, \upsilon_1) \tag{15b}$$

$$\upsilon_s(\beta^*_{1,2}) = \upsilon_2 + \upsilon_1 = f_\upsilon(\rho_1, \phi, \upsilon_1) + \upsilon_1 \tag{15c}$$

$$\upsilon_s(\beta^*_{2,2}) = \upsilon_2 + \upsilon_2 = 2\upsilon_2 \tag{15d}$$

(15) shows that the peak position of the velocity dimension is determined by the target radial velocity υ_1, the initial radial distance of the target ρ_1 and the angle ϕ. Substituting (14) into (10), we find that the peak phase is related to the target parameters ρ_1, ϕ.

In summary, the output characteristics can be determined by three parameters ρ_1, υ_1, and ϕ. Furthermore, if these three parameters are known, we can compensate the differences between channels and complete the multi-channel coherent fusion.

IV. Multi-channel fusion

In this section, a multi-channel fusion algorithm based on geometric information is proposed. Specifically, according to the geometric information as shown in Fig. 1, the searching motion parameters with respect to ρ_1, ρ_2, υ_1 and υ_2 could be mapped to the ρ_1, υ_1 and ϕ, where the explicit mathematical expression is shown in (12) and (13). Parameters ρ_1, υ_1 and ϕ are used to calculate the extracted coordinates of each channel,

and the signal energy is extracted from the four-channel RFT output. Then, a phase compensation filter is established to eliminate the phase difference between the channels and complete the coherent fusion.

A. Search Sequence Construction

First, construct the search sequence $\rho_s(\alpha_1), \upsilon_s(\beta_1)$ and $\phi_s(\gamma)$ as the input of the algorithm, where $\rho_s(\alpha_1)$ and $\upsilon_s(\beta_1)$ represents the searching initial radial distance and radial velocity from the target to node 1, $\phi_s(\gamma)$ represents the searching observation angle of radar node 1. The searching angle range and step size $\Delta\phi$ can be determined according to the system accuracy requirements. The maximum searching scope $\phi_s(\gamma) \in (0, 180^\circ)$ and number of points are N_ϕ =round$(180/\Delta\phi)$, at this time search sequence can be expressed as

$$\rho_s(\alpha_1) = -r_{\max}/2 + \alpha_1\Delta\rho/2, \qquad \alpha_1 = 1, ..., N_\rho \quad (16a)$$

$$\upsilon_s(\beta_1) = -\upsilon_{\max}/2 + \beta_1\Delta\upsilon/2, \qquad \beta_1 = 1, ..., N_\upsilon \quad (16b)$$

$$\phi_s(\gamma) = \gamma\Delta\phi, \qquad \gamma = 1, ..., N_\alpha \quad (16c)$$

B. Extraction Coordinate Calculation and Signal Extraction

Extraction coordinates $(\rho_s(\alpha_{n,m}), \upsilon_s(\beta_{n,m}))$ rule the positions to be extracted in the RFT domain of each channel

$$\begin{cases} \rho_s(\alpha_{n,m}) = \rho_s(\alpha_n) + \rho_s(\alpha_m) \\ \upsilon_s(\beta_{n,m}) = \upsilon_s(\beta_n) + \upsilon_s(\beta_m) \end{cases}, \quad n, m = 1, 2 \quad (17)$$

where $\rho_s(\alpha_{n,m})$ are the coordinates extracted for the range dimension, and $\upsilon_s(\beta_{n,m})$ are the coordinates extracted for the speed dimension. Through the analysis in section II-A, we can indirectly compute $\rho_s(\alpha_2)$ and $\upsilon_s(\beta_2)$ using the search parameters $\rho_s(\alpha_1)$, $\upsilon_s(\beta_1)$, and $\phi_s(\gamma)$. Substitute (12) and (13) into equations (16), we derive

$$\rho_s(\alpha_{1,1}) = -\rho_{\max} + \alpha_1\Delta\rho \quad (18a)$$

$$\rho_s(\alpha_{2,1}) = -\rho_{\max}/2 + \alpha_1\Delta\rho/2 + \kappa \quad (18b)$$

$$\rho_s(\alpha_{1,2}) = -\rho_{\max}/2 + \alpha_1\Delta\rho/2 + \kappa \quad (18c)$$

$$\rho_s(\alpha_{2,2}) = 2\kappa \quad (18d)$$

where

$$\kappa = \sqrt{\rho_s(\alpha_1)^2 + d^2 - 2d\gamma\Delta\phi\rho_s(\alpha_1)} \quad (19)$$

(18) are the extracted coordinates of the range dimension of each channel.

$$\upsilon_s(\beta_{1,1}) = -\upsilon_{\max} + \beta_1\Delta_\upsilon \quad (20a)$$

$$\upsilon_s(\beta_{2,1}) = -\upsilon_{\max}/2 + \beta_1\Delta_\upsilon/2\zeta \quad (20b)$$

$$\upsilon_s(\beta_{1,2}) = -\upsilon_{\max}2 + \beta_1\Delta_\upsilon/2\zeta \quad (20c)$$

$$\upsilon_s(\beta_{2,2}) = \beta_1\Delta_\upsilon\zeta \quad (20d)$$

where

$$\zeta = \frac{\cos\left(\gamma\Delta\phi + \cos^{-1}\left(\frac{\rho_s(\alpha_1) - d\gamma\Delta\phi}{\sqrt{\rho_s(\alpha_1)^2 + d^2 - 2d\gamma\Delta\phi\rho_s(\alpha_1)}}\right)\right)}{\cos(\gamma\Delta\phi)} \quad (21)$$

(20) are the extracted coordinates of the velocity dimension of each channel. Then the RFT domain extraction result of the $(m^t\text{-}n^r)$ channel can be obtained using the extracted coordinates

$$\begin{aligned} &\Omega'_{n,m}(\rho_s(\alpha_1), \upsilon_s(\beta_1), \phi_s(\gamma)) \\ &= \sum_{q=1}^{Q} E\mathrm{sinc}\left(\left(\begin{array}{l} \rho_s(\alpha_{n,m}) - \rho_s(\alpha^*_{n,m}) \\ +\left(\upsilon_s(\beta_{n,m}) - \upsilon_s(\beta^*_{n,m})\right) t_q \end{array}\right)/2\rho_r\right) \\ &\times \exp\left(-j2\pi t_q\left(\upsilon_s(\beta_{n,m}) - \upsilon_s(\beta^*_{n,m})\right)/\lambda\right) \\ &\times \exp\left(-j2\pi f_m\rho_s(\alpha^*_{n,m})/c\right) \end{aligned} \quad (22)$$

C. Phase Compensation and Coherent Fusion

To achieve coherent fusion, the phase difference term in (22) needs to be compensated. Based on (10), the phase compensation filter bank along $(m^t\text{-}n^r)$ channel can be created as follows

$$h^p_{n,m} = \exp(j2\pi f_m \cdot \rho_s(\alpha_{n,m})/c) \quad (23)$$

then the multi-channel coherent fusion output results can be obtained as follows

$$\begin{aligned} &O(\rho_s(\alpha_1), \upsilon_s(\beta_1), \phi_s(\gamma)) \\ &= \sum_{n,m=1}^{2} \Omega'_{n,m}(\rho_s(\alpha_1), \upsilon_s(\beta_1), \phi_s(\gamma)) \times h^p_{n,m} \\ &= \sum_{n,m=1}^{2}\sum_{q=1}^{Q} E\mathrm{sinc}\left(\left(\begin{array}{l} \rho_s(\alpha_{n,m}) - \rho_s(\alpha^*_{n,m}) \\ +\left(\upsilon_s(\beta_{n,m}) - \upsilon_s(\beta^*_{n,m})\right) t_q \end{array}\right)/2\rho_r\right) \\ &\times \exp\left(-j2\pi t_q\left(\upsilon_s(\beta_{n,m}) - \upsilon_s(\beta^*_{n,m})\right)/\lambda\right) \\ &\times \exp\left(-j2\pi f_m\left(\rho_s(\alpha_{n,m}) - \rho_s(\alpha^*_{n,m})\right)/c\right) \end{aligned} \quad (24)$$

The extracted coordinates of the RFT domain of each channel are equivalent to the channel peak coordinates when the search parameters match the target parameters, then the multi-channel coherent fusion output result of (24) can be simplified

$$\begin{aligned} &O(\rho_s(\alpha_1), \upsilon_s(\beta_1), \phi_s(\gamma)) \\ &= \sum_{n,m=1}^{2}\sum_{q=1}^{Q} E\sin c(0)\exp(0)\exp(0) = 4QE \end{aligned} \quad (25)$$

Based on the above fusion results, we can perform constant false alarm rate (CFAR) detection.

V. Numerical Experiments and Analysis

In this section, we first evaluate the fusion performence of the proposed algorithm in the noise-free scenario and then compare it with the MTD, KT [12], RFT [14] and method of [17] under low SNR via numerical experiments. Then, the detection performance comparison of different fusion algorithms is provided and analyzed. Finally, we discuss and compare the computational complexity between the proposed algorithm and the method of [17]. The simulation parameters are seted as 5MHz bandwidth, 0.2GHz carrier frequency, [75.00km, 75.18km] initial radial distance, [390.63 m/s, 406.25 m/s] initial radial velocity, 0.75 km node interval, 100 us pulse width, 20 ms pulse repetition interval, 5 MHz step frequency and 128 pulse number, respectively.

A. Fusion Performence Evaluation

1) Noise-free Scenario: In the noise-free scenario, firstly, the coupling echo is matched and separated, and the results are shown in Fig. (2). It could be seen that the target energy is spread over different range cells on account of the high-speed movement between the target and the MIMO radar, RM occurs at this time. To streamline the subsequent fusion performance analysis, the matching separation results are normalized.

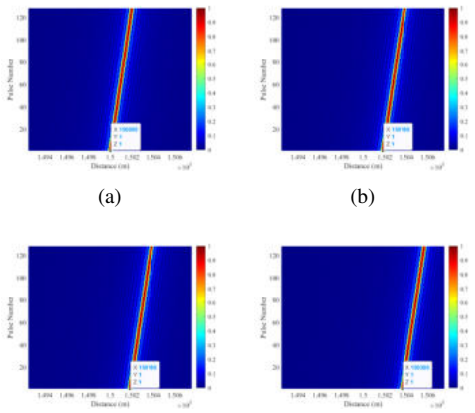

(a) (b) (c) (d)

Fig. 2. The results matched and separated from the received coupling echo, (a) (1^t-1^r) channel, (b) (1^t-2^r) channel, (c) (2^t-1^r) channel, (d)(2^t-2^r) channel.

The RFT is used to complete multi-pulse fusion. The results of Fig. (3) show that the energy of the target is successfully focused in the ρ-υ plane, the fusion peak is 128, which fuses all the pulses within the CPI, and each channel's motion parameters at the peak coordinates match the theoretical parameters.

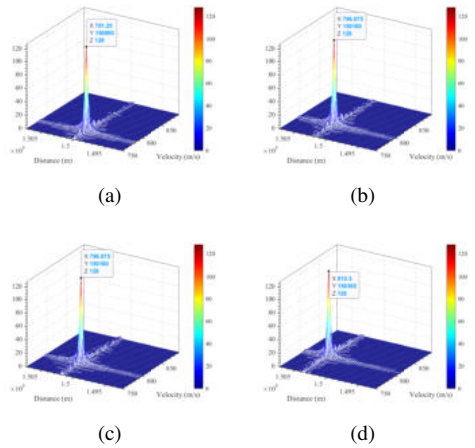

(a) (b) (c) (d)

Fig. 3. The results after multi-pulse fusion processing, (a) (1^t-1^r) channel, (b) (1^t-2^r) channel, (c) (2^t-1^r) channel, (d)(2^t-2^r) channel.

As shown in Fig. (4), the multi-channel RFT results are successfully fused using the proposed fusion algorithm. The peak value after the proposed algorithm is 512, and the theoretical peak after four-channel coherent fusion is 512, indicating that there is no energy loss during the multi-channel fusion process. Fig. (4) are the slices of the proposed algorithm output in each dimension.

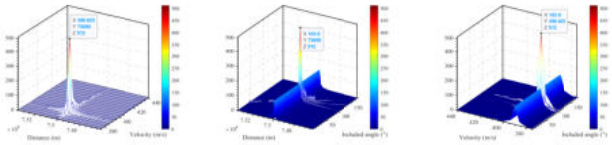

(a) (b) (c)

Fig. 4. The output of the proposed algorithm under different dimension slices, (a) range-velocity (ρ-υ) dimension, (b)range-angle (ρ-ϕ) dimension, (c) velocity-angle (υ-ϕ) dimension.

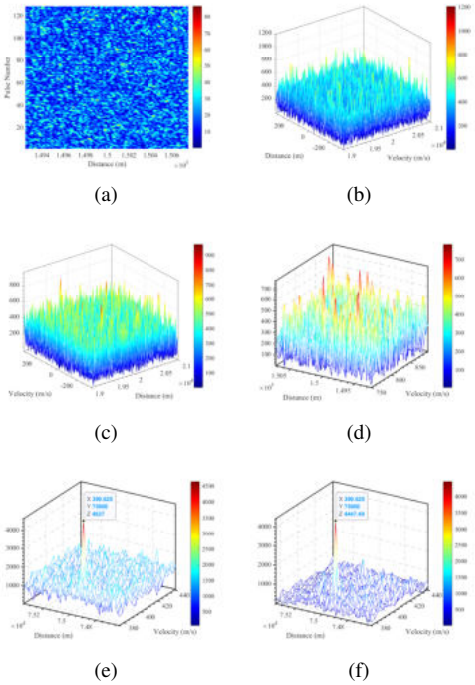

(a) (b) (c) (d) (e) (f)

Fig. 5. Fusion results of different algorithms under low SNR ratio, (a) Matching separation result, (b) MTD result, (c) KT result, (d) RFT result, (e) Method of [17], (f) Proposed algorithm.

2) Low SNR Scenario: In this section, the fusion of the proposed algorithm under low SNR is analyzed. The motion parameters of the target are the same as section V-A, while the SNR of the target's raw data is -15dB after matching and separation.

As can be seen from Fig. (5a), the result of matching and separation is submerged by noise because of the low SNR. In addition, Figs. (5b)-(5d) depict the fusion results obtained by using MTD, KT, and RFT algorithms, respectively. And the fusion results are still drowned by noise and difficult to detect.

Fig. (5e) is the result of the method of [17] and Fig. (5f) is the fusion result of the proposed algorithm. As can be seen from Fig. (5f), the peak obtained through our proposed algorithm closely aligns with method of [17], indicating the good fusion performance of our algorithm.

B. Detection Performance Analysis

In this section, 1000 independent simulation experiments are conducted based on the Monte Carlo method, and the false alarm probability is set as 10^{-3}. The detection performance of the proposed algorithm is compared with the MTD algorithm, KT algorithm, RFT algorithm, and method of [17]. The result of detection performance comparison is shown in Fig. (6), and we can see that:

1) The detection performance of the proposed algorithm is close to the method of [17] under the premise of reducing the complexity burden, and the SNR loss is less than 0.5 dB. Furthermore, in Section V-C, we compare the computational complexity of the two algorithms in detail.
2) Compared with KT and RFT methods, the proposed algorithm can achieve 6 dB and 4 dB SNR gains, respectively, which benefit from multi-channel signal fusion and effectively improve the detection ability at low SNR scenarios.
3) Compared with the proposed algorithm, the SNR required by the MTD algorithm is 16 dB higher. This is because MTD is not suitable for fusing the energy of high-speed targets, resulting in the worst detection performance.

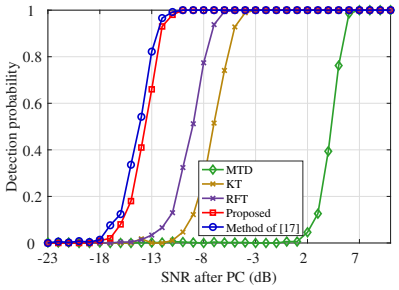

Fig. 6. Comparison of detection performance of different algorithms.

C. Computational Complexity Analysis

This section compares the computational complexity between the proposed algorithm and method of [17]. Firstly, RFT processing of single channel will be carried out $N_\rho N_\upsilon Q$ complex multiplication and $N_\rho N_\upsilon (Q-1)$ complex addition. For the method of [17], it jointly searches 4 dimensions, using $3N_\rho N_\rho N_\upsilon N_\upsilon + 4N_\rho N_\upsilon Q$ complex multiplication and $3N_\rho N_\rho N_\upsilon N_\upsilon + 4N_\rho N_\upsilon (Q-1)$ complex addition. As for the proposed algorithm, it jointly searched 3 dimensions and requires $3N_\rho N_\upsilon N_\phi + 4N_\rho N_\upsilon Q$ complex multiplication and $3N_\rho N_\upsilon N_\phi + 4N_\rho N_\upsilon (Q-1)$ complex addition. Assume that $N_\rho = N_\upsilon = N_\phi = Q = N_0$, the computational complexity of the method described in [17] is $O(N_0^4)$, in contrast, the proposed algorithm is $O(N_0^3)$. The balance between computational complexity and detection performance is achieved.

VI. Conclusion

In this paper, a multi-channel coherent fusion algorithm based on bistatic MIMO geometric information is proposed for the detection of high-speed targets. Firstly, the echo model of high-speed target is established by using the geometric space topology of radar. Then, the relationship between the single-channel fusion output and the geometric information between the radar targets is analyzed, and the corresponding phase compensation filter is designed for multi-channel coherent fusion. Finally, the proposed algorithm is compared with MTD, RFT, KT, and method of [17] through numerical experiments, which verifies that the proposed algorithm is computationally efficient.

References

[1] M. Wang, X. Li, L. Gao, Z. Sun, G. Cui, and T. S. Yeo, "Signal accumulation method for high-speed maneuvering target detection using airborne coherent MIMO radar," *IEEE Trans. Signal Process.*, vol. 71, pp. 2336-2351, 2023.

[2] X. Li et al., "STGRFT for detection of maneuvering weak target with multiple motion models," *IEEE Trans. Signal Process.*, vol. 67, no. 7, pp. 1902-1917, 1 Apr., 2019.

[3] X. Li, G. Cui, W. Yi, and L. Kong, "Coherent integration for maneuvering target detection based on Radon-Lv's distribution," *IEEE Signal Process. Lett.*, vol. 22, no. 9, pp. 1467-1471, Sept. 2015.

[4] X. Chen, J. Guan, N. Liu, and Y. He, "Maneuvering target detection via radon-fractional Fourier transform-based long-time coherent integration," *IEEE Trans. Signal Process.*, vol. 62, no. 4, pp. 939–953, Feb. 2014.

[5] J. Zheng, T. Su, W. Zhu, X. He, and Q. H. Liu, "Radar high-speed target detection based on the scaled inverse Fourier transform," *IEEE J. Sel. Topics Appl. Earth Observ. Remote Sens.*, vol. 8, no. 3, pp. 1108–1119, Mar. 2015.

[6] E. Fishler, A. Haimovich, R. Blum, D. Chizhik, L. Cimini, and R.Valenzuela, "MIMO radar: An idea whose time has come," in *Proc. IEEE Radar Conf.*, Philadelphia, PA, USA, 2004, pp. 71-78.

[7] E. Fishler, A. Haimovich, R. S. Blum, L. J. Cimini, D. Chizhik, and R. A. Valenzuela, "Spatial diversity in radars—Models and detection performance," *IEEE Trans. Signal Process.*, vol. 54, no. 3, pp. 823–838, Mar. 2006.

[8] J. Wang, W. Yi, and L. Kong, "Moving target detection in MIMO radar with asynchronous data," in *Proc. 19th Int. Conf. Inform. Fusion.*, Heidelberg, Germany, 2016, pp. 1647-1652.

[9] H. Xiao, S. Yang and W. Yi, "Weak target detection with multi-bit quantization in colocated MIMO radar," in *Proc. 24th Int. Conf. Inform. Fusion.*, Sun City, South Africa, 2021, pp. 1-6.

[10] Y.-K. Kong, B.-L. Cho, and Y.-S. Kim, "Ambiguity-free Doppler centroid estimation technique for airborne SAR using the Radon transform", *IEEE Trans. Geosci. Remote Sensing.*, vol. 43, no. 4, pp. 715–721, Apr. 2005.

[11] B. D. Carlson, E. D. Evans, and S. L. Wilson, "Search radar detection and track with the Hough transform. I. system concept", *IEEE Trans. Aerosp. Electron. Syst.*, vol. 30, no. 1, pp. 102–108, Jan. 1994.

[12] R. P. Perry, R. C. DiPietro, and R. L. Fante, "SAR imaging of moving targets", *IEEE Trans. Aerosp. Electron. Syst.*, vol. 35, no. 1, pp. 188–200, Jan. 1999.

[13] G. Li, X.-G. Xia, and Y.-N. Peng, "Doppler keystone transform: An approach suitable for parallel implementation of SAR moving target imaging," *IEEE Geosci. Remote Sens. Lett.*, vol. 5, no. 4, pp. 573–577, Oct. 2008.

[14] J. Xu, J. Yu, Y.-N. Peng, and X.-G. Xia, "Radon-Fourier transform for radar target detection, I: Generalized Doppler filter bank", *IEEE Trans. Aerosp. Electron. Syst.*, vol. 47, no. 2, pp. 1186–1202, Apr. 2011.

[15] P. Sun, J. Tang, Q. He, B. Tang, and X. Tang, "Cramer–Rao bound of parameters estimation and coherence performance for next generation radar", *IET Radar, Sonar Navigat.*, vol. 7, no. 5, pp. 553–567, Jun. 2013.

[16] C. Wang, X. Li, M. Wang, Z. Sun, and G. Cui, "Cuckoo search based noncoherent integration method for moving target detection using bistatic MIMO radar," in *Proc. IEEE Int. Conf. Signal Image Process.*, Nanjing, China, Oct. 2021, pp. 128–132.

[17] M. Wang, X. Li, Z. Zhang, G. Cui, and T. S. Yeo, "Coherent integration and parameter estimation for high-speed target detection with bistatic MIMO radar", *IEEE Trans. Geosci. Remote Sensing.*, vol. 61, pp. 1–15, 2023.